Research Square

Preprints are preliminary reports that have not undergone peer review. They should not be considered conclusive, used to inform clinical practice, or referenced by the media as validated information.

Genome wide identification and co-expression analysis of the xyloglucan endotransglucosylase/hydrolase gene family in Japanese morning glory

Kazuchika Yamauchi
Nagoya University
Katsuhiro Shiratake
shira@agr.nagoya-u.ac.jp

Nagoya University

Article

Keywords: co-expression network analysis, flower opening, genome-wide identification, Ipomoea nil, petal development, xyloglucan endotransglucosylase/hydrolase (XTH)

Posted Date: June 1st, 2026

DOI: https://doi.org/10.21203/rs.3.rs-9702690/v1

License: This work is licensed under a Creative Commons Attribution 4.0 International License. Read Full License

Additional Declarations: No competing interests reported.

Version of Record: A version of this preprint was published at Scientific Reports on October 6th, 2026. See the published version at https://doi.org/10.1038/s41598-026-73125-2.

Genome wide identification and co-expression analysis of the xyloglucan endotransglucosylase/hydrolase gene family in Japanese morning glory

Kazuchika Yamauchi and Katsuhiro Shiratake*

Graduate School of Bioagricultural Sciences, Nagoya University, Chikusa, Nagoya 464-8601, Japan

*Corresponding author : shira@agr.nagoya-u.ac.jp

Abstract

Flower opening is a dynamic process involving cell proliferation and turgor-mediated petal cell expansion. The xyloglucan endotransglucosylase/hydrolase (XTH) family enzymes are essential for these events, yet the functional roles and temporal deployment of this diverse gene family in ephemeral-flowering plant *Ipomoea nil* remains uncharacterized. In this study, 36 XTHs were identified, and their physicochemical properties and subcellular localizations were predicted, alongside organ-specific expression profiles. Furthermore, time-course transcriptomic data were utilized to

identify their specialized expression patterns through co-expression network analysis. This revealed that *InXTH* genes are organized into distinct modules synchronized with specific developmental stages. Specifically, two *InXTH* genes are highly active during the early cell-division phase, whereas five and one members are expressed immediately before and at flower opening, respectively. At these later stages, a single dominant isozyme exhibits exceptionally high transcript levels in each module, suggesting these dominant XTHs likely contribute to the cell wall remodeling required for anthesis. These findings provide fundamental insights into the temporal orchestration of cell wall-modifying enzymes and establish a molecular framework for understanding flower opening in dicots.

Keywords: co-expression network analysis, flower opening, genome-wide identification, *Ipomoea nil*, petal development, xyloglucan endotransglucosylase/hydrolase (XTH)

1. Introduction

Petal growth is initially driven by cell division and subsequently by extensive cell expansion [1]. Therefore, the rapid expansion of petal cells is a major determinant of flower size and morphology. This process is mediated by the accumulation of osmotic solutes,

37 including sugars and inorganic ions, in the vacuole, leading to an increase in intracellular
38 osmotic potential and the consequent influx of water into the cell [2]. Simultaneously, cell
39 wall loosening reduces the mechanical constraints on cell expansion, thereby allowing
40 turgor-driven cell enlargement to proceed efficiently. As a result, petal cells undergo a
41 substantial increase in volume during flower opening. Therefore, elucidating the
42 molecular and physiological mechanisms regulating solute accumulation, cell wall
43 modification, and water transport is essential for a comprehensive understanding of the
44 flower-opening process.

45 At the cellular level, this turgor-driven expansion is constrained by the rigid cell
46 wall. Mechanistically, intracellular turgor pressure drives irreversible extension of the
47 primary cell wall, resulting in cell enlargement [3]. The primary cell wall is a composite
48 network of cellulose microfibrils cross-linked by hemicellulosic polysaccharides,
49 predominantly xyloglucans in dicotyledonous plants [3]. Therefore, controlled loosening of
50 this cellulose-xyloglucan network is a prerequisite for irreversible wall extension under
51 turgor pressure [4].

52 The xyloglucan endotransglucosylase/hydrolase (XTH) family plays a central role
53 in this wall-remodeling process. XTHs catalyze endotransglucosylation (XET activity)
54 and, in some isoforms, hydrolysis (XEH activity) of xyloglucan chains, thereby

55 modulating wall extensibility and mechanics [5-7]. *XTHs* form a large multigene family in
56 higher plants, and accumulating evidence indicates isoform-specific physicochemical
57 properties, subcellular localization, and developmental regulation [8-11]. Apart from petals,
58 XTHs are broadly implicated in primary cell wall remodeling during diverse
59 developmental stages, including primary root elongation [12], root hair initiation [13], and
60 fruit softening [14].

61 Cell expansion plays an important role in flowering, particularly in petal expansion.
62 While XTHs have been reported to participate in this process in several species, such as
63 carnation [15] and osmanthus [16], a systematic, genome-wide understanding of when and
64 which distinct XTH isoforms are deployed across high-resolution developmental time
65 courses is still limited.

66 Japanese morning glory (*Ipomoea nil*) has been cultivated as a traditional
67 horticultural plant in Japan for over four centuries. Scientifically, it has been used as a
68 model plant for studying photoperiodic flowering due to its high sensitivity to day length
69 [17], as well as for investigating flower color and morphology owing to its rich genetic
70 diversity [18]. In addition, extensive genetic and genomic resources for *I. nil* have been
71 developed and maintained through the National BioResource Project (NBRP) in Japan
72 (https://shigen.nig.ac.jp/asagao/index.jsp). Beyond these classical traits, *I. nil* is

73 characterized as an ephemeral "one-day flower," where petal opening and senescence
74 occur rapidly within a daily cycle [19]. The availability of the whole genome sequence [20],
75 coupled with the recent acquisition of high-resolution time-course transcriptome data
76 covering petal development from 72 hours before to 12 hours after flowering [21], provides
77 a robust platform for molecular analysis. These extensive genomic resources, combined
78 with their dramatic physiological changes, make *I. nil* an ideal model for dissecting the
79 temporal regulation of cell wall-modifying enzymes during rapid organ expansion.

80 In this study, we performed a comprehensive genome-wide characterization of the
81 *InXTH* gene family in *I. nil*, identifying 36 genes and analyzing their phylogenetics,
82 chromosomal locations, and structural features. Furthermore, by applying weighted gene
83 co-expression network analysis (WGCNA) to transcriptomic data in petals, we identified
84 distinct gene modules corresponding to specific developmental stages. Our results
85 suggest there is a stage-specific recruitment of distinct XTH isozymes, providing new
86 insights into the transcriptional program orchestrating cell proliferation, rapid flower
87 opening, and the subsequent senescence process.

88

89 **2. Materials and methods**

90 **Identification of XTH genes in the Japanese morning glory genome**

91 To identify the XTH gene candidates in Japanese morning glory (*Ipomoea nil*),
92 BLASTP searches (e-value < 1e-10) were performed against the Japanese morning glory
93 genome database (Asagao1.2 database, http://viewer.shigen.info/asagao/) [20] and the
94 NCBI GenBank database. The amino acid sequences of *Arabidopsis thaliana* XTHs from
95 TAIR (https://www.arabidopsis.org/) [22] were used as queries.

96 The retrieved sequences and gene IDs from both databases were cross-referenced.
97 To address potential annotation errors or discrepancies observed in several genes, the
98 coding sequences were curated by comparing the genomic sequences with RNA-seq data
99 and by aligning the sequences from the two databases. These sequences were defined as
100 the putative full-length sequences of *InXTHs* for further study.

101 To verify the protein classification, the presence of the Glyco_hydro_16 domain
102 (PF00722) was confirmed using the InterProScan (https://www.ebi.ac.uk/interpro/) [23]
103 against the Pfam database [24].

104 **Physicochemical property and subcellular localization analysis**

105 The basic physicochemical properties of the identified InXTH proteins, including
106 the amino acid length, molecular weight (MW), isoelectric point (pI), and grand average
107 of hydropathy (GRAVY), were predicted using the ProtParam tool on the ExPASy server
108 (https://web.expasy.org/protparam/). For subcellular localization analysis, the presence of

109 N-terminal signal peptides and their cleavage sites were predicted using SignalP 6.0
110 (https://services.healthtech.dtu.dk/services/SignalP-6.0/) [25] with the "Eukarya" setting.
111 TargetP 2.0 (https://services.healthtech.dtu.dk/services/TargetP-2.0/) [26] with the "Plant"
112 organism group setting was used to discriminate between secretory pathway signal
113 peptides, mitochondrial transit peptides, and chloroplast transit peptides. The precise
114 subcellular location was predicted using DeepLoc 2.1
115 (https://services.healthtech.dtu.dk/services/DeepLoc-2.1/) [27].

116 **Multiple sequence alignment and phylogenetic analysis**

117 The amino acid sequences of XTHs were aligned using the CLUSTALW
118 program(https://www.genome.jp/tools-bin/clustalw), and neighbor-joining (NJ)
119 phylogenetic tree was constructed using MEGA12 [28] with the following parameters:
120 Poisson model, pairwise deletion and 1,000 bootstrap replications. The identified XTHs
121 were categorized into three subfamilies (Groups I/II, IIIA, IIIB) based on *Arabidopsis*
122 *thaliana* [10] and *Ipomoea batatas* [11].

123 **Gene structure and protein motif analysis**

124 Gene structure (exon-intron structure) was schematized using coding sequences
125 (CDSs) and genomic sequence of the *InXTH*s by the Gene Structure Display Server 2.0
126 (https://gsds.gao-lab.org/) [29]. Multiple Expectation Maximization for Motif Elicitation

127 (https://meme-suite.org/meme/tools/meme) [30] was used to identify the conserved motifs
128 in the amino acid sequences of InXTHs. The parameters were set as follows: The "zero
129 or one occurrence per sequence" (ZOOPS) model was selected for site distribution, the
130 maximum number of motifs was set to 12, and the motif width was restricted to a range
131 of 6 to 50 amino acids.

132 **Chromosomal location and gene duplication analysis**

133 Information regarding the chromosome distribution of the *InXTH* genes was
134 retrieved from the Asagao1.2 database. The chromosomal locations were visualized using
135 MapChart [31]. Tandemly duplicated genes were identified as clusters of two or more *InXTH*
136 genes located within 100 kbp of each other.

137 **Gene expression profile**

138 Gene expression data for different organs of Japanese morning glory, expressed as
139 RPKM values, were obtained from the Japanese morning glory RNA-seq database
140 (https://viewer.shigen.info/asagao/download.php).

141 Prior to analysis, the expression values for *InXTH29*, which was annotated as two
142 separate genes due to an annotation error, were corrected by calculating the length-
143 weighted average of the RPKM values to represent the expression of the single full-length
144 gene. For visualization, the RPKM values were log2-transformed [log2(RPKM + 1)] and

145 a heatmap was generated using the pheatmap R package, with hierarchical clustering
146 applied to the genes based on expression similarity.

147 Temporal gene expression data using FPKM values in petals were obtained from
148 the temporal transcriptome data and interactive database
149 (https://ipomoeanil.nibb.ac.jp/fpkm/) [21], which includes time-course transcriptome data
150 of petals at multiple stages, ranging from the pre-opening stage to the late senescence
151 stage.

152 **Weighted gene co-expression network construction analysis (WGCNA)**

153 For the construction of the co-expression network, the comprehensive FPKM
154 dataset derived from *Ipomoea nil* petals was downloaded from the DNA Data Bank of
155 Japan (DDBJ)/GEA under accession number E-GEAD-856 [21].

156 Co-expression network analysis was performed using WGCNA R package [32]. To
157 construct a robust scale-free network, we selected top 7,000 genes based on the coefficient
158 of variation of expression among all samples. In addition, 32 *InXTH* genes with detectable
159 expressions were explicitly included in the dataset, resulting in a total of 7,023 genes for
160 network construction. Soft-thresholding power of $\beta = 5$ was chosen to achieve a scale-
161 free topology fit index of 0.9. A signed network was constructed using the
162 blockwiseModules function, with a minimum module size of 30 and a merged cut height

163 of 0.25. Module membership (kME) was calculated for each *InXTH* gene as the
164 correlation between its expression profile and the module eigengene of its assigned
165 module. *InXTH* genes with kME < 0.3 were excluded from module-based analyses (n =
166 9), as they lacked reliable co-expression patterns.

167 **Visualization of module expression profile and *InXTH* gene expression**

168 To visualize the temporal expression patterns of each module, the mean Module
169 Eigengene (ME) values were plotted across time points with standard errors. The
170 expression level of *InXTH* genes within each module were evaluated using the maximum
171 FPKM value observed within the entire time course. The values were visualized as bar
172 plots, and pseudo-log10 transformation was applied to the y-axis to accommodate the
173 expression levels using the ggplot2 R package.

174

175 **3. Results**

176 **Identification and phylogenetic analysis of XTH genes in Japanese morning glory**

177 To identify the *XTH* genes of Japanese morning glory, we performed a BLASTP
178 search on the morning glory genome database (Asagao1.2 database,
179 http://viewer.shigen.info/asagao/) [20] and the NCBI GenBank database, using amino acid
180 sequences of *Arabidopsis thaliana* XTHs obtained from TAIR

181 (https://www.arabidopsis.org/) [22] as queries. In total, 37 and 42 candidates were identified
182 in the Asagao1.2 database and the NCBI GenBank database, respectively (Supplemental
183 Table S1, S2). Cross-reference of these candidates revealed several discrepancies from
184 annotation differences between the two databases. Regarding splicing variants,
185 XM_019343467.1 and XM_019343468.1 in the NCBI GenBank database were identified
186 as identical to INIL12g22043 in the Asagao1.2 database. XM_019300959.1 and
187 XM_019300960.1 were identified to be identical to INIL15g28182. Similarly, three
188 splicing variants XM_019326605.1, XM_019326606.1, and XM_019326607.1 were
189 found for INIL13g09293. The longest isoform, XM_019326605.1, was selected as the
190 representative sequence. Furthermore, XM_019337944.1 and XM_019337945.1 both
191 aligned to the exon regions of INIL03g17598, indicating potential redundancy in the
192 GenBank database. Conversely, INIL03g17601 lacked a corresponding annotation in the
193 NCBI GenBank database. For INIL13g15562, three amino acids deletion was observed
194 after residue 62 in the Asagao1.2 sequence. The deletion was manually curated based on
195 the orthologous sequence from sweet potato (*Ipomoea batatas*). Finally, comparison with
196 a single locus XM_019332083.1 revealed that INIL12g01243 and INIL12g01244 each
197 represent a fragment of a single locus, while annotated as two separate genes. Therefore,
198 the sequence from XM_019332083.1 was used for further study. A total of 36 InXTHs,

199 including the previously reported InXTH1 to InXTH4 [33], were identified (Table 1). The
200 newly identified XTHs were named InXTH5 to InXTH36, according to their gene
201 position on the chromosomes. All 36 InXTH proteins were confirmed to possess the
202 Glyco_hydro_16 domain (PF00722) by InterProScan (https://www.ebi.ac.uk/interpro/) [23]
203 analysis against the Pfam database [24]. This domain belongs to the glycoside hydrolase
204 family 16 (GH16) and serves as the core catalytic domain, containing the conserved motif
205 essential for xyloglucan endotransglucosylase and hydrolase activities [34]. Furthermore,
206 35 of these proteins were also found to possess the xyloglucan endotransglucosylase
207 (XET) C-terminus domain (PF06955).

Gene Name	Gene ID (Asagao1.2)	Gnomon (NCBI)	Sub family	Chromosome number	Position on chromosome		Strand	Source	Number of animo acids	Number of exons	Pfam ID	Molecular weight (Da)	pI	GRAVY	SignalP 6.0			TargetP 2.0	DeepLoc 2.1
					start	end									Prediction	Probability	Cleavage Site		
InXTH1	INIL10g13325	XM_019330562.1	I/II	10	11,696,949	11,700,497	-	Asagao	295	4	PF00722, PF06955	34,031	8.8	-0.348	Sec/SPI	0.9998	21-22	Signal Peptide	Extracellular (0.70)
InXTH2	INIL00g00888	XM_019328032.1	I/II	scaffold0177	202,039	204,229	-	Asagao	293	3	PF00722, PF06955	32,516	6.2	-0.323	Sec/SPI	0.9994	32-33	Signal Peptide	Extracellular (0.73)
InXTH3	INIL12g07349	XM_019324453.1	I/II	12	13,998,009	13,999,624	-	NCBI	281	3	PF00722, PF06955	32,332	9.3	-0.350	Sec/SPI	0.9997	29-30	Signal Peptide	Extracellular (0.70)
InXTH4	INIL02g40690	XM_019317605.1	I/II	2	9,532,946	9,534,570	+	Asagao	292	4	PF00722, PF06955	33,674	6.4	-0.493	Sec/SPI	0.9998	28-29	Signal Peptide	Extracellular (0.67)
InXTH5	INIL00g00887	XM_019328024.1	I/II	scaffold0177	184,048	185,992	-	NCBI	291	3	PF00722, PF06955	32,492	5.7	-0.381	Sec/SPI	0.9997	29-30	Signal Peptide	Extracellular (0.75)
InXTH6	INIL00g14642	XM_019333792.1	I/II	scaffold1161	313,088	314,604	-	NCBI	298	4	PF00722, PF06955	35,140	8.8	-0.566	Sec/SPI	0.9997	27-28	Signal Peptide	Extracellular (0.70)
InXTH7	INIL02g02171	XM_019294555.1	I/II	2	33,901,936	33,903,111	+	NCBI	292	1	PF00722, PF06955	32,684	6.6	-0.395	Sec/SPI	0.9992	27-28	Signal Peptide	Extracellular (0.79)
InXTH8	INIL02g02173	XM_019294556.1	I/II	2	33,917,163	33,918,333	-	NCBI	292	1	PF00722, PF06955	32,684	6.6	-0.395	Sec/SPI	0.9992	27-28	Signal Peptide	Extracellular (0.79)
InXTH9	INIL02g02176	XM_019294562.1	I/II	2	33,928,615	33,929,790	+	NCBI	292	1	PF00722, PF06955	32,684	6.6	-0.395	Sec/SPI	0.9992	27-28	Signal Peptide	Extracellular (0.79)
InXTH10	INIL03g17597	XM_019337942.1	I/II	3	32,711,764	32,713,103	-	Asagao	299	3	PF00722, PF06955	33,490	9.1	-0.432	Sec/SPI	0.9997	30-31	Signal Peptide	Extracellular (0.75)
InXTH11	INIL03g17598	XM_019337944.1 XM_019337945.1	I/II	3	32,714,615	32,716,053	-	Asagao	299	3	PF00722, PF06955	33,467	8.6	-0.459	Sec/SPI	0.9997	30-31	Signal Peptide	Extracellular (0.75)
InXTH12	INIL03g17599	XM_019337948.1	I/II	3	32,718,868	32,720,285	-	NCBI	289	3	PF00722, PF06955	32,460	8.5	-0.369	Sec/SPI	0.9998	23-24	Signal Peptide	Extracellular (0.86)
InXTH13	INIL03g17601		I/II	3	32,734,342	32,735,783	-	Asagao	177	3	PF00722	19,733	5.9	-0.195	Sec/SPI	0.9996	23-24	Signal Peptide	Extracellular (0.80), Lysosome/Vacuole (0.60)
InXTH14	INIL03g17602	XM_019337956.1	I/II	3	32,737,842	32,738,933	-	Asagao	287	2	PF00722, PF06955	32,301	8.2	-0.414	Sec/SPI	0.9998	23-24	Signal Peptide	Extracellular (0.87)
InXTH15	INIL03g17603	XM_019337947.1	I/II	3	32,744,541	32,745,703	-	Asagao	292	2	PF00722, PF06955	32,922	7.0	-0.414	Sec/SPI	0.9998	24-25	Signal Peptide	Extracellular (0.87)
InXTH16	INIL03g17604	XM_019337946.1	I/II	3	32,749,050	32,750,212	+	NCBI	292	2	PF00722, PF06955	32,951	8.2	-0.395	Sec/SPI	0.9998	23-24	Signal Peptide	Extracellular (0.88)
InXTH17	INIL03g17764	XM_019338506.1	I/II	3	34,207,885	34,210,097	-	NCBI	306	4	PF00722, PF06955	35,001	6.8	-0.355	Sec/SPI	0.6206	27-28	Signal Peptide	Extracellular (0.65)
InXTH18	INIL04g02467	XM_019299450.1	IIIA	4	12,530,243	12,532,227	-	NCBI	300	4	PF00722, PF06955	34,611	9.0	-0.474	Sec/SPI	0.9998	23-24	Signal Peptide	Endoplasmic reticulum (0.55)
InXTH19	INIL04g28594	XM_019301646.1	I/II	4	32,446,559	32,451,843	+	Asagao	295	3	PF00722, PF06955	33,002	7.0	-0.324	Sec/SPI	0.9998	29-30	Signal Peptide	Extracellular (0.65)
InXTH20	INIL04g34954	XM_019309641.1	I/II	4	1,564,920	1,567,128	+	Asagao	296	4	PF00722, PF06955	33,356	5.0	-0.172	Sec/SPI	0.9997	23-24	Signal Peptide	Extracellular, Lysosome/Vacuole (0.79)
InXTH21	INIL04g34955	XM_019309987.1	I/II	4	1,567,640	1,570,350	+	Asagao	298	4	PF00722, PF06955	34,837	9.2	-0.176	Other(No SP detected)	0.5807		Signal Peptide	Extracellular (0.56)
InXTH22	INIL05g22414	XM_019344243.1	I/II	5	29,377,303	29,379,377	-	NCBI	290	4	PF00722, PF06955	33,408	5.5	-0.410	Sec/SPI	0.9997	25-26	Signal Peptide	Extracellular (0.83)
InXTH23	INIL07g14095	XM_019333400.1	IIIA	7	11,597,027	11,600,543	+	NCBI	314	4	PF00722, PF06955	35,524	7.2	-0.492	Sec/SPI	0.9997	39-40	Signal Peptide	Extracellular (0.57)
InXTH24	INIL07g14097	XM_019333399.1	IIIA	7	11,655,388	11,657,487	+	NCBI	318	4	PF00722, PF06955	35,715	8.4	-0.493	Sec/SPI	0.979	43-44	Signal Peptide	Endoplasmic reticulum (0.53)
InXTH25	INIL08g04613	XM_019321204.1	IIIB	8	4,841,872	4,844,486	-	Asagao	334	4	PF00722, PF06955	37,839	7.7	-0.416	Sec/SPI	0.9888	20-21	Signal Peptide	Extracellular (0.60)
InXTH26	INIL08g13761	XM_019332833.1	I/II	8	10,981,180	10,983,355	+	NCBI	289	4	PF00722, PF06955	32,960	8.2	-0.444	Sec/SPI	0.9998	23-24	Signal Peptide	Extracellular (0.83)
InXTH27	INIL09g30467	XM_019303302.1	I/II	9	3,114,472	3,116,389	-	Asagao	280	4	PF00722, PF06955	31,484	5.5	-0.367	Other(No SP detected)	1		Other	Extracellular (0.92)
InXTH28	INIL10g12149	XM_019330706.1	IIIA	10	315,435	317,640	+	NCBI	332	4	PF00722, PF06955	37,733	9.2	-0.243	Other(No SP detected)	0.9137		Signal Peptide	Extracellular (0.53)
InXTH29	INIL12g01243,INIL12g01244	XM_019332083.1	IIIB	12	2,736,493	2,739,321	+	NCBI	346	4	PF00722, PF06955	39,799	6.8	-0.572	Sec/SPI	0.9998	25-26	Signal Peptide	Extracellular (0.68)
InXTH30	INIL12g22043	XM_019343467.1 XM_019343468.1	IIIA	12	59,622,390	59,624,490	-	Asagao	295	4	PF00722, PF06955	33,552	8.5	-0.560	Sec/SPI	0.9998	20-21	Signal Peptide	Extracellular (0.70)
InXTH31	INIL13g09293	XM_019326605.1 XM_019326606.1 XM_019326607.1	I/II	13	8,743,628	8,746,101	+	Asagao	343	5	PF00722, PF06955	39,640	8.7	-0.485	Other(No SP detected)	1		Other	Endoplasmic reticulum (0.66), Golgi apparatus (0.74)
InXTH32	INIL13g15562	XM_019335353.1	IIIB	13	12,326,135	12,330,237	-	Asagao *	319	4	PF00722, PF06955	36,768	8.8	-0.444	Sec/SPI	0.9998	22-23	Signal Peptide	Extracellular (0.65)
InXTH33	INIL13g39072	XM_019315482.1	IIIB	13	32,800,299	32,802,344	+	Asagao	315	4	PF00722, PF06955	35,570	8.4	-0.278	Sec/SPI	0.9997	31-32	Signal Peptide	Extracellular (0.70)
InXTH34	INIL14g03989	XM_019319025.1	I/II	14	3,944,452	3,946,439	+	Asagao	302	4	PF00722, PF06955	35,006	5.2	-0.508	Sec/SPI	0.9998	28-29	Signal Peptide	Extracellular (0.71)
InXTH35	INIL14g42001	XM_019318842.1	I/II	14	53,250,426	53,251,878	+	Asagao	282	3	PF00722, PF06955	32,265	7.0	-0.385	Sec/SPI	0.9997	27-28	Signal Peptide	Extracellular (0.75)
InXTH36	INIL15g28182	XM_019300959.1 XM_019300960.1	I/II	15	6,127,150	6,128,820	+	Asagao	292	4	PF00722, PF06955	33,323	8.2	-0.288	Sec/SPI	0.9996	27-28	Signal Peptide	Extracellular (0.85)

209 To identify relationships of the identified InXTHs, a neighbor-joining (NJ)
210 phylogenetic tree was constructed using MEGA12 [28] (Fig. 1). A total of 36 InXTH protein
211 sequences from morning glory, 36 IbXTH protein sequences from sweet potato [11] and 33
212 AtXTH protein sequences from Arabidopsis [10] were used to verify the subfamily
213 classification. The topology of the phylogenetic tree was consistent with the established
214 subfamily classifications from previous studies, showing no major discrepancies.
215 Subfamily I/II was the largest group, containing 27genes. This subfamily included all four
216 previously reported *InXTH* genes (*InXTH1–4*). The remaining were classified into
217 Subfamily IIIA (5 genes) and Subfamily IIIB (4 genes).

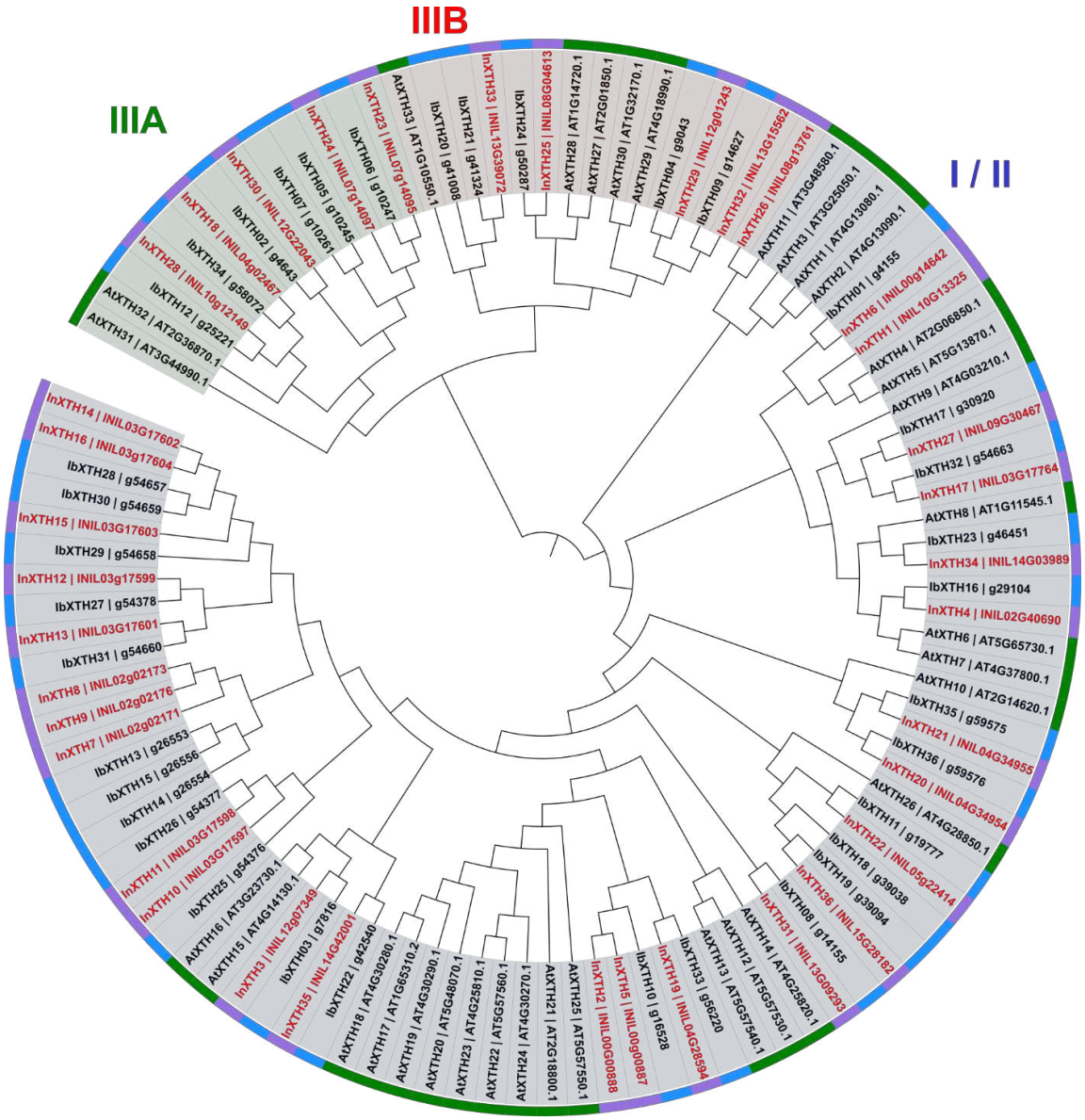

Figure1. Phylogenetic tree of the XTHs of *Ipomoea nil, I. batatas* and *Arabidopsis thaliana* . The phylogenetic tree was constructed using the Neighbor-Joining (NJ) method based on the alignment of full-length amino acid sequences of XTHs from *I. nil* (InXTHs), *I. batatas* (IbXTHs), and *A. thaliana* (AtXTHs). Color strips indicate the species of origin: purple for *I. nil*, blue for *I. batatas*, and green for *A. thaliana*. Background colors distinguish between the three major XTH subfamilies (Group I/II: light blue; Group IIIA: light green; Group IIIB: pink).

226 **Gene structure and protein motif of InXTHs**

227 Gene structures (exon-intron structures) of *InXTHs* were visualized by the Gene

228 Structure Display Server 2.0 (https://gsds.gao-lab.org/) [29] based on their coding sequences

229 (CDSs) and genomic sequences. While *InXTH* genes in Subfamily I/II contained 1 to 4

230 exons, all genes in Subfamily IIIA and IIIB possessed 4 exons (Fig. 2a).

231 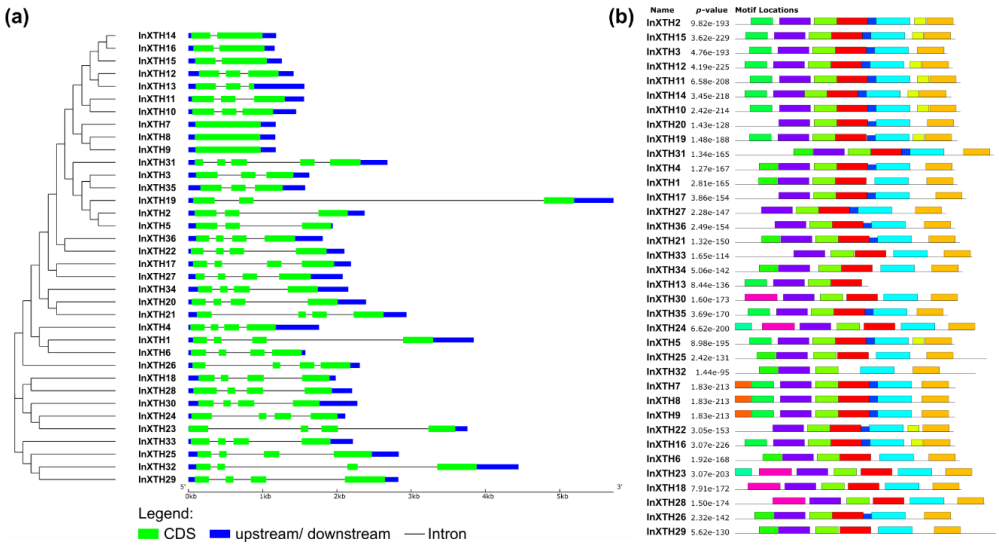

232 **Figure 2. Gene structure and conserved protein motifs of the *InXTHs*.**

233 **(a)** Exon-intron organization of *InXTH* genes. Green boxes, black lines, and blue boxes represent
234 exons, introns, and untranslated regions (UTRs), respectively. **(b)** Distribution of conserved
235 motifs in InXTH proteins identified by MEME analysis. Each colored box represents a distinct
236 motif.

237

238 To characterize the InXTH proteins, conserved protein motifs were determined

239 using MEME suite (https://meme-suite.org/meme/tools/meme) [30], and 12 conserved

240 motifs were identified (Fig. 2b). Most of the XTHs showed highly conserved motifs in

241 the same order. Among the 12 motifs, Motif 8 was exclusively found in Subfamily IIIA
242 proteins.

243 **Chromosomal distribution and gene duplication of *InXTH*s**

244 The chromosomal distribution of 36 *InXTH* genes was visualized using MapChart
245 [31] (Fig. 3). A total of 33 *InXTH* genes were mapped onto the 15 pseudo-chromosomes,
246 while the remaining three genes (*INIL00g00887*, *INIL00g00888*, and *INIL00g14642*)
247 were located on scaffolds. The distribution of *InXTH* genes revealed an uneven
248 distribution of *InXTH* genes across the chromosomes. Chr.3 harbored the largest number
249 of *InXTHs* (8 genes), followed by Chr.2 and Chr.4 with 4 genes each. Conversely, Chr.1,
250 Chr.6, and Chr.11 did not harbor any *InXTH* gene.

251 Tandem duplications of *InXTHs* in the morning glory were estimated based on the
252 criteria established by Huang et al. (2012) [35], as two or more homologous genes within a
253 100 kbp distance. Using this criteria, five clusters of tandem duplicated *InXTHs* were
254 identified. These included a three-gene cluster on Chr.2 (*INIL02g02171*, *INIL02g02173*,
255 and *INIL02g02176*); the largest cluster comprising seven genes on Chr.3 (*INIL03g17597*,
256 *INIL03g17598*, *INIL03g17599*, *INIL03g17601*, *INIL03g17602*, *INIL03g17603*,
257 *INIL03g604*); and two-gene clusters on Chr.4 (*INIL04g34954*, *INIL04g34955*), two and

258 Chr.7 (*INIL07g14095*, *INIL07g14097*). Additionally, one cluster was identified on

259 scaffold0177 (*INIL00g00887*, *INIL00g00888*).

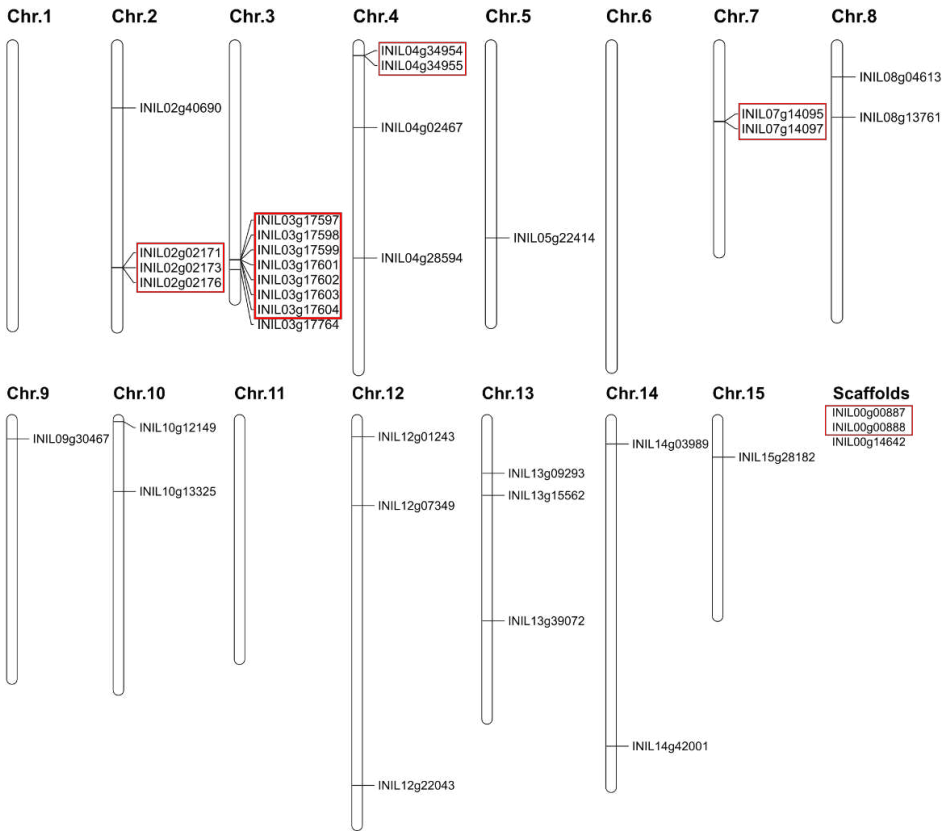

260

261 **Figure 3. Chromosomal distribution of the *InXTH* genes.**

262 The physical locations of 36 *InXTH* genes were mapped onto the 15 chromosomes and
263 unanchored scaffolds of *I. nil* based on the Asagao Genome Database. Thirty-three genes are
264 located on chromosomes, while three are situated on scaffolds. Red boxes indicate gene clusters
265 resulting from duplication events. The map was generated using MapChart.

266

267 **Protein property and subcellular localization of InXTHs**

268 The physicochemical properties of the 36 identified InXTH proteins are listed in

269 Table 1. The amino acid sequences ranged from 177 (InXTH13) to 346 (InXTH29)

270 residues, with molecular weight (MW) spanning from 19.7 to 39.8 kDa. The theoretical

271 isoelectric points (pI) showed a broad distribution from 5.0 (InXTH20) to 9.3 (InXTH3),
272 indicating diversity in the electrostatic properties of the family members. The Grand
273 Average of Hydropathicity (GRAVY) values were consistently negative for all InXTH
274 proteins, indicating their hydrophilic nature.

275 Regarding subcellular localization, SignalP 6.0 [25] predicted that 32 of the 36 InXTH
276 proteins (88.9%) possess an N-terminal signal peptide (Sec/SPI). The prediction
277 probabilities for the cleavage sites were high (>0.99) for the majority of these proteins.
278 TargetP 2.0 [26] and DeepLoc 2.1 [27] classified 30 of these signal peptide-containing proteins
279 as extracellular, consistent with the predictions from SignalP 6.0. Some proteins exhibited
280 localization scores for the endoplasmic reticulum (ER), Golgi apparatus or vacuoles.
281 Among the four proteins classified as lacking a signal peptide by SignalP 6.0 (InXTH21,
282 InXTH27, InXTH28, and InXTH31), two (InXTH21 and InXTH28) were predicted to
283 possess a signal peptide by TargetP 2.0 and were classified as extracellular by DeepLoc
284 2.1. The remaining two InXTHs (InXTH27 and InXTH31) consistently lacked signal
285 peptide predictions across multiple tools.

286 **Gene expression profile of *InXTHs* in different organs**

287 To elucidate the organ-specific expression patterns of *InXTH* genes, we analyzed
288 RNA-seq data covering six organs (root, stem, leaf, flower, seed coat, and embryo)
289 obtained from the Asagao1.2 database. The gene expression profiles of all 36 *InXTHs*
290 were visualized in a heatmap (Fig. 4). A gene was considered expressed if its RPKM value
291 exceeded 0.5, a threshold consistent with the preprocessing parameters used for the
292 subsequent WGCNA. The total expression levels of *InXTH* genes varied among organs.
293 The highest total RPKM was observed in stems and roots, followed by flowers and seed
294 coats, with the lowest expression levels in leaves and embryos. Expression levels also
295 varied by subfamily classification. Genes in Subfamily I/II generally exhibited expression
296 across multiple organs. In contrast, Subfamilies IIIA and IIIB showed specific expressions
297 among the organs. Within Subfamily IIIA, only three genes (*InXTH23*, *InXTH28*, and
298 *InXTH30*) showed detectable expression. Similarly, in Subfamily IIIB, only *InXTH25*
299 exceeded the detection threshold.

300 Based on the RPKM threshold (> 0.5), seven genes (*InXTH1*, *InXTH3*, *InXTH10*,
301 *InXTH16*, *InXTH17*, *InXTH27,* and *InXTH34*) were identified as constitutively expressed
302 across all analyzed organs. The previously reported genes *InXTH1–4* exhibited high
303 expression not only in flowers but also in stems and roots, implying that they play a

304 constitutive role in cell expansion throughout plant development. Conversely, five genes
305 (*InXTH5*, *InXTH6*, *InXTH18*, *InXTH24,* and *InXTH31*) exhibited RPKM values below
306 0.5 in all organs, suggesting potential pseudogenization or specific expression under
307 specific conditions.

308 Regarding organ specificity, distinct expression patterns were observed in flowers
309 and the seed coat. Three tandemly duplicated genes (*InXTH7*, *InXTH8*, and *InXTH9*)
310 exhibited flower specific expression. These genes showed high expression (RPKM > 150)
311 in flowers, while their expression levels remained below the threshold (RPKM < 0.5) in
312 other organs. Additionally, *InXTH20* exhibited specific expression in the seed coat,
313 accounting for approximately half of the total *XTH* expression in this organ.

314 Furthermore, we examined the expression divergence within tandemly duplicated
315 gene clusters identified in the chromosomal analysis. A marked expression divergence
316 was observed in the *InXTH2*, *InXTH5* tandem pair. While *InXTH2* was highly expressed
317 especially in roots, its paralog *InXTH5* showed no expression across all organs. A contrast
318 in expression profiles was also found in the putative tandem pair *InXTH20* and *InXTH21*.
319 While *InXTH20* was predominantly expressed in the seed coat, its paralog *InXTH21*
320 exhibited only weak expression in roots, stems, and flowers, suggesting functional
321 differentiation. In the *InXTH10–InXTH16* cluster, *InXTH10* and *InXTH16* showed

constitutive expression, whereas other members showed restricted expression. Collectively, these contrasting expression profiles suggest that tandemly duplicated *InXTH* genes have acquired distinct transcriptional regulation, leading to their functional divergence following duplication events.

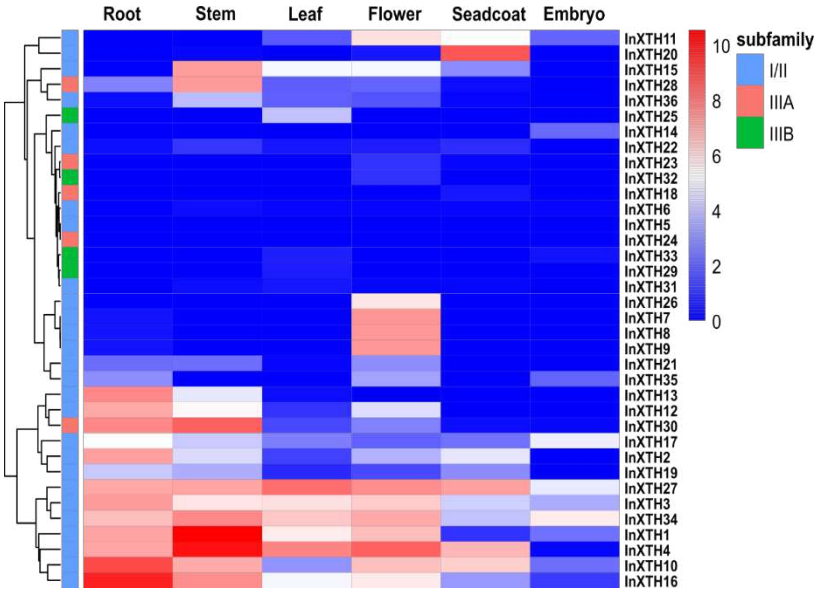

Figure 4. Tissue-specific gene expression profiles of the *InXTHs*.
Heatmap visualization of *InXTH* gene expression across various organs based on RNA-seq data from the Asagao Genome Database. Gene expression levels are presented as log2-transformed RPKM values [log2(RPKM +1)]. Genes (rows) are clustered hierarchically based on expression similarity, while tissues (columns) are arranged in anatomical order. The color scale ranges from blue (low expression) to red (high expression). Note that for *InXTH29*, which is annotated as two separate fragments in the database, RPKM values represent the length-weighted average of the fragments to correct for this annotation error.

Gene expression profile of *InXTHs* during petal development and senescence

To elucidate functions of InXTHs in petal, including development of petal, flower opening and closing, the temporal gene expressions of *InXTHs* in petal was profiled

339 utilizing the time-course transcriptome database for Japanese morning glory petals by
340 Nakagawa et al. [21] (Fig. 5). Within Subfamily I/II members, *InXTH4* exhibited the highest
341 expression among all *InXTH* genes, with a maximum FPKM value exceeding 18,000 (Fig.
342 5a). Transcript levels increased during the dark period prior to anthesis and reached a
343 peak at the time of flower opening (0 h). *InXTH1* also showed high expression (maximum
344 FPKM > 7,000) but displayed a different temporal pattern, peaking 3 h before flower
345 opening. While other Subfamily I/II members were detected, their expression levels were
346 substantially lower compared to the dominant *InXTH4* and *InXTH1*.

347 Genes in Subfamily IIIA generally showed low expression throughout the examined
348 period (Fig. 5b). Specific temporal patterns were detected, such as a gradual decrease in
349 *InXTH28* from 72 h before flower opening and a minor peak in *InXTH30* at 6 h post-
350 flowering. However, their absolute expression levels remained low. In contrast, within
351 Subfamily IIIB, only *InXTH29* exhibited a distinct expression peak (Fig. 5c). It reached
352 a maximum FPKM exceeding 600 at 6 h before flower opening, whereas other genes
353 remained at negligible levels.

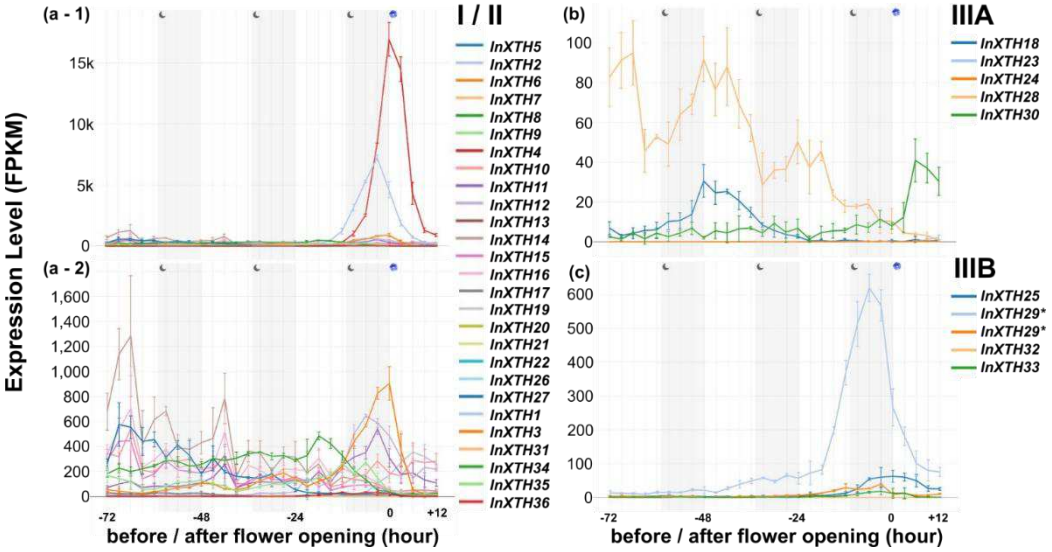

Figure 5. Gene expression profiles of the *InXTHs* in the petals before and after flower opening.

Gene expression patterns of the *InXTH*s were obtained from the temporal transcriptome data and interactive database (https://ipomoeanil.nibb.ac.jp/fpkm/). The plots display the expression levels (FPKM) from 3-h interval from 72 h before and 12 h after flower opening. (a-1) Full scale plots of Group I/II subfamily. (a-2) A magnified view of (a-1) focusing on genes with lower expression levels. (b) Group IIIA subfamily. (c) Group IIIB subfamily. Each line corresponds to an individual *InXTH* gene. Note that *InXTH29* is represented by two separate lines due to split gene annotation in the database.

Weighted gene co-expression network analysis (WGCNA)

To elucidate the gene regulatory networks associated with *InXTHs,* we performed a WGCNA using the time-course transcriptome data. To ensure the robustness of the network, we first optimized the number of genes included in the analysis by evaluating the scale-free topology fit index (R^2) across datasets with varying numbers of high-CV (coefficient of variation) genes. The subset of the top 7,000 variable genes yielded the optimal scale-free topology using a soft-thresholding power of β=5. By combining these

372 high-CV genes with 32 *InXTH* genes that showed detectable expression (FPKM > 0.5), a
373 total of 7,023 genes were subjected to the analysis. Hierarchical clustering based on
374 topological overlap identified 24 distinct co-expression modules, which varied widely in
375 size from 49 to 2,838 genes (Supplemental Fig. S1). To assess the reliability of module
376 assignments for *InXTH* genes, module membership (kME) was calculated for each gene
377 as the correlation with its assigned module eigengene. Nine *InXTH* genes with kME < 0.3
378 were excluded from subsequent module-based analyses, as they did not exhibit reliable
379 co-expression patterns. The 23 *InXTH* genes were distributed across six modules:
380 turquoise (n = 6), blue (n = 3), brown (n = 1), yellow (n = 2), red (n = 10), and grey (n =
381 1). The grey module comprises genes that could not be assigned to any specific co-
382 expression cluster.

383 Analysis of module eigengenes revealed distinct temporal trends across the
384 identified modules (Fig. 6). The blue module exhibited a gradual decrease in expression
385 starting approximately 69 h before flower opening. Transitioning toward anthesis, the red
386 module showed a peak between 6 and 3 h before flower opening, followed by the yellow
387 module, which peaked at the time of flower opening (0 h). In the post- flower opening
388 phase, the brown module exhibited a peak at 3 h, whereas the turquoise module showed
389 a continuous increasing trend after the brown module.

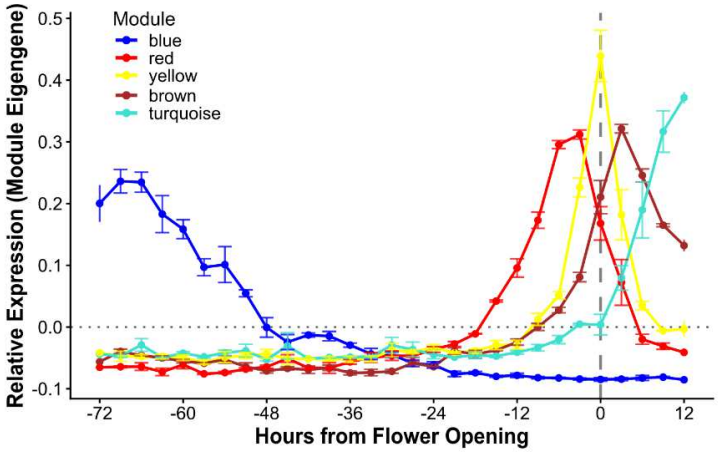

Figure 6. Temporal gene expression profiles of co-expression modules identified by WGCNA. Profiles of module eigengenes for the five selected modules (blue, red, yellow, brown, and turquoise) during petal development. The x-axis represents the time in hours relative to flower opening (0 h; indicated by the vertical dashed line). The y-axis represents the module eigengene value, indicating the relative expression pattern of each module. Data points and lines indicate the mean values, and error bars represent the standard error (SE) of biological replicates (n = 3).

Functional characterization of *InXTH* co-expression modules

To clarify the biological functions of each module in WGCNA, we next analyzed the expression profiles and intramodular connectivity (k_{ME}) of the constituent genes. Figure 7 summarizes the maximum expression levels of the *InXTH* genes assigned to the five key modules (blue, red, yellow, brown, and turquoise). Based on these profiles, we identified hub genes characterized by high connectivity ($k_{ME} > 0.8$) and expression levels (Supplemental Table S3). Additionally, Gene Ontology (GO) enrichment analysis was performed to characterize the biological processes associated with each module (Supplemental Fig. S2).

407 The blue module exhibited a distinct temporal profile, peaking at 69 to 66 h before
408 flower opening, decreasing to 48 h, and maintaining a low basal level thereafter.
409 Consistent with this trend, the module was significantly enriched in GO terms related to
410 "cell division" and "cell cycle." Notably, *InXTH27* (k_{ME} = 0.80) was identified as a highly
411 expressed hub gene within this cluster. This downregulation pattern matches the cessation
412 of cell division activity at approximately 48 h before anthesis as reported previously [21].
413 Consequently, *InXTH27* expression is temporally correlated with the cell proliferation
414 phase.

415 The red module (peaking 3–6 h before anthesis) and the yellow module (peaking at
416 0 h) exhibited contrasting expression patterns regarding *XTH* genes. The red module was
417 characterized by the coordinated expression of multiple *InXTH* genes. *InXTH1* was
418 identified as a highly expressed hub gene (k_{ME} = 0.93), co-expressed with *InXTH12*,
419 *InXTH29*, *InXTH33*, and *InXTH36*, along with cell wall-modifying enzymes such as
420 pectinesterase. This indicates that a specific subset of XTH isozymes and cell wall
421 enzymes are transcriptionally co-regulated prior to flower opening.

422 In contrast, the yellow module was predominantly driven by a single *XTH* gene,
423 *InXTH4*. *InXTH4* showed the highest expression level among the *InXTH* family members
424 (Max FPKM > 18,000) and appeared as a dominant hub (k_{ME} = 0.84), co-expressed with

425 auxin-responsive genes like *SAUR72* and *SAUR50-like*. This implies that the rapid petal
426 expansion at anthesis is not orchestrated by a diverse set of *XTHs*, but rather by the robust
427 induction of *InXTH4*.

428 The brown module, which peaked 3 h after flower opening, contained putative
429 epigenetic regulators, including *histone H2A* and *methyl-CpG-binding domain-*
430 *containing protein 6*. The presence of these factors indicates that the expression of
431 chromatin remodeling components temporally coincides with the transition from open
432 flower to the onset of senescence. In the brown module, *InXTH2* (k_{ME} = 0.90) was
433 identified as a highly expressed hub gene.

434 The turquoise module, showing an increasing trend after flower opening, contained
435 genes associated with protein degradation and transcriptional regulation, such as *SKP1-*
436 *like proteins* and *WRKY transcription factor 75*. Six *InXTH* genes were assigned to this
437 module and co-expressed with these senescence-associated hubs. The expression pattern
438 is consistent with the progression of petal wilting, implicating a subset of InXTHs in the
439 senescence process.

440

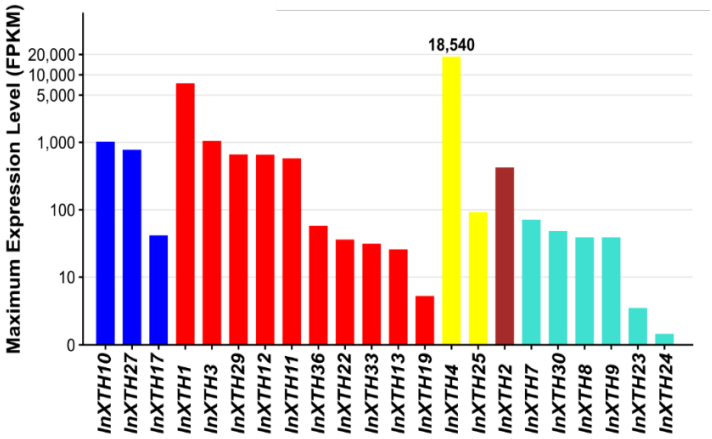

Figure 7. Maximum expression levels of *InXTH* genes across co-expression modules. The bar chart displays the maximum expression level (FPKM) recorded for each *InXTH* gene across the entire developmental time course. Genes are grouped by their assigned WGCNA modules (blue, red, yellow, brown, and turquoise) and sorted within each module in descending order. The y-axis is presented on a pseudo-logarithmic. Bar colors correspond to the module colors. Numerical labels indicate the exact FPKM values for genes showing exceptionally high expression (>10,000 FPKM).

4. Discussion

The identification of 36 *InXTH* genes in the *I. nil* genome highlighted an expansion of the *XTH* gene family in the *I. nil* compared to other plants (Fig. 1). The subfamily distribution in I. nil (Group I/II: 27, IIIA: 5, IIIB: 4) is largely comparable to that of its close relative, *I. batatas* (Group I/II: 25, IIIA: 6, IIIB: 5) [11]. However, the slight increase in Group I/II members in I. nil suggests that lineage-specific gene duplications have occurred after the divergence of these two species, contributing to the distinct evolutionary path of the *I. nil* genome.

458 Chromosomal distribution analysis revealed that *InXTH* genes are unevenly
459 distributed, forming five distinct clusters (Fig. 3). Notably, the largest cluster on Chr.3
460 contains seven *XTH* genes within a narrow physical distance. This genomic organization
461 mirrors the arrangement observed in *I. batatas*, where a major *XTH* cluster is located on
462 Chr.13 [11], suggesting that these clusters originated from a common ancestor prior to
463 speciation. Interestingly, phylogenetic analysis revealed a complex evolutionary history
464 for these clustered genes, in which some *InXTH* members formed orthologous pairs with
465 *IbXTHs*, whereas others formed paralogous clades solely within *I. nil*. This pattern
466 suggests that the expansion of the *InXTH* family resulted from a combination of ancient
467 segmental duplications shared by the genus *Ipomoea* and recent, lineage-specific tandem
468 duplications specific to *I. nil*. Consequently, the gene cluster on Chr.3 appears to be a
469 major site of such duplication events, which likely contributed to the functional
470 diversification of the family.

471 XTH enzymes function in the apoplast for cell wall remodeling [5]. Secretion of these
472 proteins to the apoplast typically requires an N-terminal signal peptide [36]. Consistent with
473 this expectation, our analysis showed that most InXTHs (88.9%) contained a predicted
474 signal peptide and are classified as extracellular, supporting their expected roles in cell
475 expansion (Table. 1). However, a few InXTHs showed atypical localization predictions.

476 Predicted localization to the ER or Golgi apparatus may reflect transient residence within
477 the conventional secretory pathway. The absence of a predicted signal peptide in
478 InXTH27 and InXTH31 may have resulted from misannotation of the start codon, or
479 potentially atypical secretion mechanisms. Although most cell wall proteins are secreted
480 via the conventional signal peptide–dependent pathway, non-canonical cell wall proteins
481 lacking signal peptides have occasionally been reported [36]. However, such proteins are
482 often considered potential contaminants in cell wall proteomic analyses, and their
483 extracellular localization requires careful validation.

484 Regarding transcriptional regulation, our comprehensive profiling (Fig. 4 and 5)
485 revealed that *InXTH* expression patterns are not strictly correlated with their phylogenetic
486 classification (Fig. 1). Genes belonging to different subfamilies exhibited expression
487 peaks mostly around anthesis and during senescence. This observation suggests that the
488 transcriptional regulation of *XTH* genes has evolved independently of their coding
489 sequences. Rather than being constrained by subfamily identity, distinct *XTH* genes
490 appear to have been recruited to function at specific developmental stages, such as flower
491 opening and senescence. This divergence in expression patterns is indicative of
492 subfunctionalization, allowing distinct isozymes to specialize in specific developmental
493 phases. Consequently, distinct *XTH* isozymes appear to be deployed at different

494 developmental phases, likely contributing to the precise cell wall remodeling required for
495 petal morphogenesis.

496 This study revealed that the expression of *InXTH* genes is not uniform throughout
497 petal development but is orchestrated in a distinct, stage-specific manner (Fig. 6). Among
498 the co-expression modules identified by WGCNA, we focused on five *InXTH*-containing
499 modules that correspond to specific developmental phases, including cell proliferation in
500 the blue module, preparation for anthesis in the red module, rapid expansion in the yellow
501 module, and the transition to senescence in the brown and turquoise modules
502 (Supplemental Fig. S2). These findings suggest that distinct XTH isozymes are recruited
503 to fulfill specific cell wall remodeling requirements at each developmental stage, rather
504 than being mediated by a single enzyme handling the entire process.

505 The blue module, represented by *InXTH27*, exhibited preferential transcript
506 accumulation until 48 h before flower opening (Fig. 6). This period coincides with the
507 active cell division phase in *I. nil* petals [21]. While XTH family enzymes are most widely
508 documented for their roles in facilitating cell wall loosening during rapid cell expansion
509 [34], the specific temporal correlation of *InXTH27* with the proliferation phase implies a
510 distinct physiological function. This isozyme likely contributes to the cell wall
511 remodeling required for cytokinesis or the post-mitotic enlargement of daughter cells [37] .

512 Given that the primary cell wall must be dynamic to accommodate cell plate formation
513 [4,38], *InXTH27* may facilitate the structural modification of the nascent wall network. This
514 hypothesis is supported by a recent finding that specific Arabidopsis *XTH* members,
515 *AtXTH4* and *AtXTH7*, are essential for callus proliferation during graft union formation
516 [39]. Phylogenetically, *InXTH17* and *InXTH27* belong to the broader clade which includes
517 these proliferation-associated *AtXTHs*. Coupled with their transcript accumulation during
518 the early development stages, this phylogenetic similarity implies that these blue module
519 *InXTHs* possibly share a conserved function regarding cell wall plasticity for active cell
520 division.

521 Immediately prior to flower opening (-6 to -3 h), the red module was characterized
522 by the concurrent upregulation of multiple *InXTH* genes alongside a cell wall-modifying
523 enzyme (*pectinesterase*) and a *potassium transporter* (Supplemental Table S3 and Fig. 6).
524 Specifically, the presence of *InXTH1* in this pre-opening phase is consistent with previous
525 findings that *InXTH1* expression is closely correlated with petal elongation [33].The co-
526 expression of different *XTH* subfamilies implies that isozymes with distinct enzymatic
527 properties may act in a complementary manner to facilitate effective cell wall loosening
528 and remodeling [34]. Furthermore, the presence of *pectinesterase* suggests that modification
529 of the pectin matrix occurs in parallel with xyloglucan remodeling, likely to modulate the

530 cell wall mechanical properties for the impending expansion [40]. In addition, the
531 upregulation of the *potassium transporter* indicates that solute accumulation begins prior
532 to full opening, priming the cells for the turgor-driven expansion that follows[41].

533 The yellow module, peaking at the time of flower opening, was dominated by the
534 robust expression of *InXTH4* (Fig.6, 7). Considering the ephemeral nature of the one-day
535 flower of *I. nil*, in which full opening occurs rapidly within a limited time [21], these results
536 suggest that *InXTH4* acts as a principal driver of this rapid petal unfolding. This result is
537 consistent with the previous study by Shinozaki et al. (2014), which identified *InXTH4* as
538 a key gene whose expression dictates the rate of flower opening under different
539 photoperiods [33]. Notably, this module also contained two co-expressed SAUR (small
540 auxin upregulated RNA) genes (Supplemental Table S3). SAUR proteins are established
541 effectors of the acid growth mechanism, promoting cell elongation through the activation
542 of H^+-ATPases and consequent apoplastic acidification [42]. The synchronized gene
543 expression of *InXTH4* and *SAUR* supports the hypothesis that auxin-mediated apoplastic
544 acidification could create a favorable environment for *InXTH4* activity [8], thereby
545 facilitating the substantial cell expansion observed at anthesis.

546 Following anthesis, the brown module, which peaked at 3 h after flower opening,
547 showed the upregulation of several putative epigenetic regulators, including genes

548 annotated as *histone H2A* and *methyl-CpG-binding domain proteins* (Supplemental Table
549 S3and Fig. 6). This timing coincides with the transition from the fully open state to the
550 onset of petal wilting. The induction of these chromatin-associated factors suggests that
551 transcriptional reprogramming may occur at this stage, potentially contributing to the
552 repression of growth-associated genes and the initiation of senescence-related pathways
553 [43].

554 Subsequently, the turquoise module, which increased during wilting, was enriched
555 in hubs associated with protein degradation, e.g., *SKP1-like proteins*, and transcriptional
556 regulation (Supplemental Table S3 and Fig. 6). A prominent hub was *WRKY75*, a
557 transcription factor known to act as a positive regulator of senescence in Arabidopsis [44].
558 The co-expression of specific *InXTH* genes within this module suggests that cell wall
559 modification or disassembly accompanies the senescence program, possibly facilitating
560 nutrient remobilization from degenerating petal organs to plant body. Therefore, the
561 expression profile of this module is consistent with transcriptomic evidence showing that
562 autophagy-related and transporter genes are coordinately upregulated during petal
563 senescence, supporting nutrient remobilization [21].

564 Collectively, the time-resolved co-expression analysis reveals a sequential
565 transcriptional program in which distinct XTH isozymes are engaged at successive stages

566 of petal development, coupling cell wall remodeling to cell proliferation, rapid expansion

567 at anthesis, and ordered disassembly during senescence.

568

569 **References**

570 1 van Doorn, W. & van Meeteren, U. Flower opening and closure: a review. *JOURNAL OF*
571 *EXPERIMENTAL BOTANY* **54**, 1801-1812 (2003). https://doi.org/10.1093/jxb/erg213
572 2 Yamada, K., Norikoshi, R., Suzuki, K., Imanishi, H. & Ichimura, K. Determination of
573 subcellular concentrations of soluble carbohydrates in rose petals during opening by
574 nonaqueous fractionation method combined with infiltration-centrifugation method. *PLANTA*
575 **230**, 1115-1127 (2009). https://doi.org/10.1007/s00425-009-1011-6
576 3 Cosgrove, D. Growth of the plant cell wall. *NATURE REVIEWS MOLECULAR CELL*
577 *BIOLOGY* **6**, 850-861 (2005). https://doi.org/10.1038/nrm1746
578 4 Fry, S. Primary cell wall metabolism: tracking the careers of wall polymers in living plant
579 cells. *NEW PHYTOLOGIST* **161**, 641-675 (2004). https://doi.org/10.1111/j.1469-
580 8137.2004.00980.x
581 5 Rose, J., Braam, J., Fry, S. & Nishitani, K. The XTH family of enzymes involved in
582 xyloglucan endotransglucosylation and endohydrolysis: current perspectives and a new
583 unifying nomenclature. *PLANT AND CELL PHYSIOLOGY* **43**, 1421-1435 (2002).
584 https://doi.org/10.1093/pcp/pcf171
585 6 Nishitani, K. & Tominaga, R. Endoxyloglucan transferase, a novel class of
586 glycosyltransferase that catalyzes transfer of a segment of xyloglucan molecule to another
587 xyloglucan molecule. *JOURNAL OF BIOLOGICAL CHEMISTRY* **267**, 21058-21064 (1992).
588 7 Desilva, J. *et al.* Molecular characterization of a xyloglucan-specific endo-(1-]4)-beta-D-
589 glucanase (xyloglucan endotransglycosylase) from nasturtium seeds. *PLANT JOURNAL* **3**,
590 701-711 (1993).
591 8 Maris, A. *et al.* Differences in enzymic properties of five recombinant xyloglucan
592 endotransglucosylase/hydrolase (XTH) proteins of Arabidopsis thaliana. *JOURNAL OF*
593 *EXPERIMENTAL BOTANY* **62**, 261-271 (2011). https://doi.org/10.1093/jxb/erq263
594 9 Yokoyama, R. & Nishitani, K. A comprehensive expression analysis of all members of a gene
595 family encoding cell-wall enzymes allowed us to predict cis-regulatory regions involved in
596 cell-wall construction in specific organs of arabidopsis. *PLANT AND CELL PHYSIOLOGY*
597 **42**, 1025-1033 (2001). https://doi.org/10.1093/pcp/pce154

10 Yokoyama, R., Rose, J. & Nishitani, K. A surprising diversity and abundance of xyloglucan endotransglucosylase/hydrolases in rice. Classification and expression analysis. *PLANT PHYSIOLOGY* **134**, 1088-1099 (2004). https://doi.org/10.1104/pp.103.035261

11 Zhang, J. *et al.* Genome-wide identification and expression analysis of the xyloglucan endotransglucosylase/hydrolase gene family in sweet potato [Ipomoea batatas (L.) Lam]. *INTERNATIONAL JOURNAL OF MOLECULAR SCIENCES* **24** (2023). https://doi.org/10.3390/ijms24010775

12 Osato, Y., Yokoyama, R. & Nishitani, K. A principal role for AtXTH18 in Arabidopsis thaliana root growth: a functional analysis using RNAi plants. *JOURNAL OF PLANT RESEARCH* **119**, 153-162 (2006). https://doi.org/10.1007/s10265-006-0262-6

13 Vissenberg, K., Fry, S. & Verbelen, J. Root hair initiation is coupled to a highly localized increase of xyloglucan endotransglycosylase action in arabidopsis roots. *PLANT PHYSIOLOGY* **127**, 1125-1135 (2001). https://doi.org/10.1104/pp.127.3.1125

14 Han, Y. *et al.* Isolation and characterization of two persimmon xyloglucan endotransglycosylase/hydrolase (XTH) genes that have divergent functions in cell wall modification and fruit postharvest softening. *FRONTIERS IN PLANT SCIENCE* **7** (2016). https://doi.org/10.3389/fpls.2016.00624

15 Harada, T. *et al.* Cloning, characterization, and expression of xyloglucan endotransglucosylase/hydrolase and expansin genes associated with petal growth and development during carnation flower opening. *JOURNAL OF EXPERIMENTAL BOTANY* **62**, 815-823 (2011). https://doi.org/10.1093/jxb/erq319

16 Yang, Y. *et al.* Genome-wide identification and expression analysis of XTH gene family during flower-opening stages in Osmanthus fragrans. *PLANTS-BASEL* **11** (2022). https://doi.org/10.3390/plants11081015

17 Hayama, R., Agashe, B., Luley, E., King, R. & Coupland, G. A circadian rhythm set by dusk determines the expression of FT homologs and the short-day photoperiodic flowering response in Pharbitis. *PLANT CELL* **19**, 2988-3000 (2007). https://doi.org/10.1105/tpc.107.052480

18 Morita, Y. & Hoshino, A. Recent advances in flower color variation and patterning of Japanese morning glory and petunia. *BREEDING SCIENCE* **68**, 128-138 (2018). https://doi.org/10.1270/jsbbs.17107

19 Shibuya, K., Shimizu, K., Niki, T. & Ichimura, K. Identification of a NAC transcription factor, EPHEMERAL1, that controls petal senescence in Japanese morning glory. *PLANT JOURNAL* **79**, 1044-1051 (2014). https://doi.org/10.1111/tpj.12605

20 Hoshino, A. *et al.* Genome sequence and analysis of the Japanese morning glory Ipomoea nil. *Nature Communications* **7**, 13295 (2016). https://doi.org/10.1038/ncomms13295

21 Nakagawa, S. *et al.* Transcriptomic dynamics of petal development in the one-day flower species, Japanese morning glory (Ipomoea nil). *PLANT AND CELL PHYSIOLOGY* **66**, 1823-1838 (2025). https://doi.org/10.1093/pcp/pcaf108

22 Berardini, T. *et al.* The arabidopsis information resource: Making and mining the "gold standard" annotated reference plant genome. *GENESIS* **53**, 474-485 (2015). https://doi.org/10.1002/dvg.22877

23 Paysan-Lafosse, T. *et al.* InterPro in 2022. *NUCLEIC ACIDS RESEARCH* **51**, D418-D427 (2023). https://doi.org/10.1093/nar/gkac993

24 Mistry, J. *et al.* Pfam: The protein families database in 2021. *NUCLEIC ACIDS RESEARCH* **49**, D412-D419 (2021). https://doi.org/10.1093/nar/gkaa913

25 Teufel, F. *et al.* SignalP 6.0 predicts all five types of signal peptides using protein language models. *NATURE BIOTECHNOLOGY* **40**, 1023-+ (2022). https://doi.org/10.1038/s41587-021-01156-3

26 Armenteros, J. *et al.* Detecting sequence signals in targeting peptides using deep learning. *LIFE SCIENCE ALLIANCE* **2** (2019). https://doi.org/10.26508/lsa.201900429

27 Odum, M. *et al.* DeepLoc 2.1: multi-label membrane protein type prediction using protein language models. *NUCLEIC ACIDS RESEARCH* **52**, W215-W220 (2024). https://doi.org/10.1093/nar/gkae237

28 Kumar, S. *et al.* MEGA12: Molecular evolutionary genetic analysis version 12 for adaptive and green computing. *MOLECULAR BIOLOGY AND EVOLUTION* **41** (2024). https://doi.org/10.1093/molbev/msae263

29 Hu, B. *et al.* GSDS 2.0: an upgraded gene feature visualization server. *BIOINFORMATICS* **31**, 1296-1297 (2015). https://doi.org/10.1093/bioinformatics/btu817

30 Bailey, T., Johnson, J., Grant, C. & Noble, W. The MEME Suite. *NUCLEIC ACIDS RESEARCH* **43**, W39-W49 (2015). https://doi.org/10.1093/nar/gkv416

31 Voorrips, R. MapChart: Software for the graphical presentation of linkage maps and QTLs. *JOURNAL OF HEREDITY* **93**, 77-78 (2002). https://doi.org/10.1093/jhered/93.1.77

32 Langfelder, P. & Horvath, S. WGCNA: an R package for weighted correlation network analysis. *BMC BIOINFORMATICS* **9** (2008). https://doi.org/10.1186/1471-2105-9-559

33 Shinozaki, Y. *et al.* Length of the dark period affects flower opening and the expression of circadian-clock associated genes as well as xyloglucan endotransglucosylase/hydrolase genes in petals of morning glory (Ipomoea nil). *PLANT CELL REPORTS* **33**, 1121-1131 (2014). https://doi.org/10.1007/s00299-014-1601-z

34 Eklof, J. & Brumer, H. The XTH gene family: an update on enzyme structure, function, and phylogeny in xyloglucan remodeling. *PLANT PHYSIOLOGY* **153**, 456-466 (2010). https://doi.org/10.1104/pp.110.156844

35 Huang, S. *et al.* Genome-wide analysis of WRKY transcription factors in Solanum lycopersicum. *MOLECULAR GENETICS AND GENOMICS* **287**, 495-513 (2012). https://doi.org/10.1007/s00438-012-0696-6

36 Jamet, E., Canut, H., Boudart, G. & Pont-Lezica, R. Cell wall proteins: a new insight through proteomics. *TRENDS IN PLANT SCIENCE* **11**, 33-39 (2006). https://doi.org/10.1016/j.tplants.2005.11.006

37 Matsui, A. *et al.* AtXTH27 plays an essential role in cell wall modification during the development of tracheary elements. *PLANT JOURNAL* **42**, 525-534 (2005). https://doi.org/10.1111/j.1365-313X.2005.02395.x

38 Jürgens, G. Cytokinesis in higher plants. *ANNUAL REVIEW OF PLANT BIOLOGY* **56**, 281-299 (2005). https://doi.org/10.1146/annurev.arplant.55.031903.141636

39 Xiong, M. *et al.* Xyloglucan endotransglucosylase/hydrolase family genes are required for the plant graft union formation through callus proliferation. *PLANT PHYSIOLOGY* **200** (2026). https://doi.org/10.1093/plphys/kiag030

40 Wolf, S. & Greiner, S. Growth control by cell wall pectins. *PROTOPLASMA* **249**, 169-175 (2012). https://doi.org/10.1007/s00709-011-0371-5

41 Shabala, S. & Lew, R. Turgor regulation in osmotically stressed Arabidopsis epidermal root cells. Direct support for the role of inorganic ion uptake as revealed by concurrent flux and cell turgor measurements. *PLANT PHYSIOLOGY* **129**, 290-299 (2002). https://doi.org/10.1104/pp.020005

42 Spartz, A. *et al.* SAUR inhibition of PP2C-D phosphatases activates plasma membrane H+-ATPases to promote cell expansion in Arabidopsis. *PLANT CELL* **26**, 2129-2142 (2014). https://doi.org/10.1105/tpc.114.126037

43 Feng, S. *et al.* DNA methylation remodeled amino acids biosynthesis regulates flower senescence in carnation (Dianthus caryophyllus). *NEW PHYTOLOGIST* **241**, 1605-1620 (2024). https://doi.org/10.1111/nph.19499

44 Guo, P. *et al.* A tripartite amplification loop involving the transcription factor WRKY75, salicylic acid, and reactive oxygen species accelerates leaf senescence. *PLANT CELL* **29**, 2854-2870 (2017). https://doi.org/10.1105/tpc.17.00438

Acknowledgements

This work was supported by JSPS KAKENHI Grant Numbers 24K01745 and 21H02184.

Funding

This work was supported by JSPS KAKENHI Grant Numbers 24K01745 and 21H02184.

Data Availability

The genomic data analyzed in this study are publicly available in the Japanese morning glory genome database (Asagao1.2 database, http://viewer.shigen.info/asagao/) and NCBI database under accession number BDFN00000000.1. The datasets generated during the analysis are available from the corresponding author on reasonable request.

Contributions

K.Y. and K.S. conceived the study and designed the study. K.Y. performed the bioinformatic analyses and wrote the manuscript. K.S. reviewed and edited the manuscript and supervised the project. All authors reviewed and approved the final manuscript.

Corresponding author

Correspondence to Katsuhiro Shiratake.

Competing interests

The authors declare no competing interests.

723 **Supplementary information**

724 **Table S1.** List of InXTH candidate genes identified in the Ipomoea nil genome database

725 (Asagao1.2).

726 **Table S2.** List of InXTH candidate genes identified in the NCBI GenBank database.

727 **Table S3.** Hub genes identified in the five key co-expression modules based on module

728 membership (kME > 0.8) and expression levels.

729 **Figure S1.** Hierarchical clustering dendrogram of expressed genes identified by WGCNA.

730 **Figure S2.** Gene Ontology (GO) enrichment analysis of the co-expression modules.

731

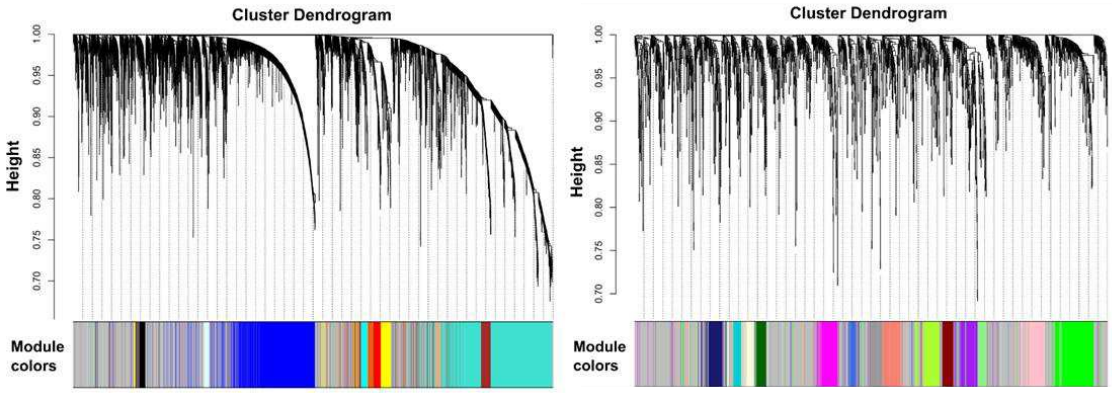

732

733 **Supp Figure S1. Hierarchical clustering dendrogram of expressed genes identified by**
734 **WGCNA.**
735 The dendrogram was constructed based on the co-expression similarity (topological overlap) of
736 expressed genes across the developmental stages of *I. nil* petals. Each vertical branch (leaf) in the
737 tree represents an individual gene. The colored row below the dendrogram indicates the specific
738 co-expression module to which each gene was assigned by the dynamic tree cut algorithm.

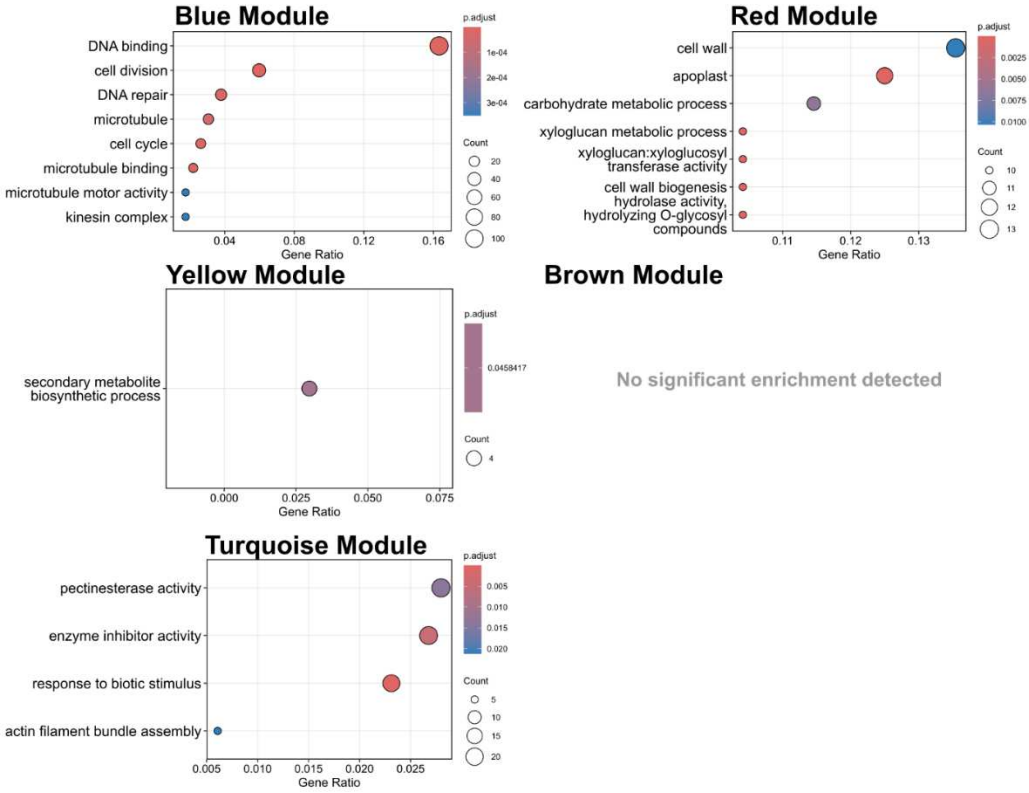

Supp Figure S2. Gene Ontology (GO) enrichment analysis of the co-expression modules. Dot plots showing the top significantly enriched GO terms for the genes assigned to the blue, red, yellow, turquoise, and brown modules identified by WGCNA. The enrichment analysis was performed using the clusterProfiler R package based on a custom gene-to-GO term mapping dataset. To ensure analytical accuracy, obsolete GO terms were excluded using the GO.db package prior to the enrichment test. All genes filtered for the WGCNA were used as the background universe. The statistical significance of enrichment was defined by a Benjamini-Hochberg (BH) adjusted P-value < 0.05. The color gradient of the dots represents the adjusted P-value, while the size of the dots corresponds to the number of genes (Count) associated with each GO term. The x-axis indicates the GeneRatio (the proportion of module genes associated with a specific term relative to the total number of annotated genes in that module). Note that no significantly enriched GO terms were detected for the brown module.